GEOLOGICA CARPATHICA, 2026, 77, 3, 205–221 https://doi.org/10.31577/GeolCarp.2026.09

Whole-rock and Sr–Nd isotope geochemistry of Paleozoic metabasic rocks from southern Menderes Massif, western Türkiye: Geotectonic implications

CİHAN ÇOLAK[1,✉] and ALİ KAYA[1]

[1]Pamukkale University, Faculty of Engineering, Department of Geological Engineering, TR 20160 Denizli, Türkiye

(Manuscript received October 6, 2025; accepted in revised form April 28, 2026; Associate Editor: Igor Broska)

Abstract: This study investigates the metabasic rocks forming the core series of the southern Menderes Massif (MM) within the Anatolide–Tauride Block (ATB). In the Babadağ (Denizli) region, these rocks are exposed as sills and stocks intruding the schist units, and are classified as amphibolite, garnet amphibolite, and hornblende gabbro. The metabasic rocks of the southern MM provide important insights into regional geotectonic evolution through major and trace element geochemistry, rare earth element (REE) systematics, and Sr–Nd isotope analyses. These rocks typically display similar mineral assemblages, with widespread retrograde metamorphism and hydrothermal alteration, while primary magmatic textures are locally preserved, especially in hornblende gabbros. Geochemical classification based on immobile element systematics indicates that the metabasic rocks are derived from magmatic protoliths and display transitional alkaline–tholeiitic characteristics, predominantly plotting in the alkali basalt field and partly overlapping the tholeiitic basalt field. Variation diagrams of major and trace elements reveal systematic fractionation, controlled by the removal of clinopyroxene, olivine, and spinel, as reflected by decreasing CaO/Al_2O_3 ratios, Ni (60–511 ppm), and Cr (22–1265 ppm) concentrations with declining MgO contents (6.07–14.85 wt.%). The enrichment of incompatible elements such as TiO_2, Y, Zr, and Th further supports the cogenetic relationship of these rocks and indicates fractional crystallization from a common parental magma. Primitive mantle-normalized multi-element patterns display enrichment relative to N-MORB and transitional signatures between E-MORB and OIB, with a dominant OIB-like affinity. Chondrite-normalized REE patterns are characterized by strong LREE enrichment ($(La/Yb)_{cn}$=5–16) and nearly flat HREE profiles, suggesting melt generation within the spinel–garnet transition zone. The Sr–Nd isotopic compositions (measured) ($^{87}Sr/^{86}Sr$=0.706633–0.710964; $^{143}Nd/^{144}Nd$=0.512518–0.51267), together with mantle-like Nb/U (16–63) and low Ce/Pb (1.9–7.6) ratios, point to an enriched and compositionally heterogeneous mantle source. Tectonic discrimination diagrams indicate that the magmatism took place in an intraplate extensional setting related to Paleo-Tethyan lithospheric extension along the northern margin of Gondwana.

Keywords: intraplate magmatism, asthenospheric mantle, OIB-like

Introduction

The Alpine–Himalayan orogenic belt stands as a geological record of the prolonged interactions between Gondwana and Laurasia, chronicling the effects of multiple Tethyan oceanic cycles over time. Stretching from the Carpathians and Balkans through Anatolia, this orogenic corridor reflects key events such as the opening of the Paleo-Tethys Ocean, the rifting and northward migration of continental fragments derived from Gondwana, and the subsequent evolution and closure of the Neo-Tethys (Şengör & Yilmaz 1981; Şengör 1984; Şengör et al. 1984b; Stampfli & Borel 2002; Stampfli et al. 2013).

Plate tectonic reconstructions suggest that the Paleo-Tethys Ocean emerged between Gondwana and Laurasia during the late Paleozoic, gradually subducting beneath the southern edge of Eurasia (Stampfli et al. 2013). The closure of this ancient ocean was marked by processes such as subduction, accretion, and crustal thickening, remnants of which are variably preserved in the basement rocks and associated tectonic units across southeastern Europe and Anatolia (Okay et al. 2006; Schmid et al. 2020). With plate reorganization during the Triassic, ribbon-shaped continental blocks broke away from northern Gondwana, leading to the formation of the Neo-Tethys Ocean and a major reconfiguration of the Tethyan domain (Şengör 1984; Şengör et al. 1984b; Stampfli & Borel 2002; Stampfli et al. 2013; Şengör et al. 2023).

In regions like the Carpathians and the Balkans, structural and stratigraphic evidence provides constraints on both the timing and geometry of Paleo-Tethyan subduction and the succeeding stages of Mesozoic convergence. These records preserve the complex, multi-phase tectonic evolution that resulted from the ongoing interplay between Gondwana-derived continental slivers and the Eurasian margin (Schmid et al. 2020; van Hinsbergen et al. 2020 and references therein). Further southeast, Anatolia serves as a critical transitional area, where continental fragments of diverse paleogeographic origins were amalgamated during repeated episodes of ocean opening and closure. The Anatolian Plate itself contains several prominent suture zones, which are remnants of various Tethyan oceanic realms and chronicle successive events of subduction,

✉ corresponding author: Cihan Çolak
chn.clk@outlook.com

accretion, and continental collision (Okay & Tüysüz 1999). Altogether, this intricate tectonic framework reveals the patchwork assembly of continental blocks with different origins, reflecting the prolonged and dynamic evolution of the Tethyan region (Bozkurt & Mittwede 2001).

The Paleozoic evolution of the northern Gondwanan margin and its connection to the Paleo-Tethyan realm has been interpreted through various geodynamic models. Within this framework, deposition within the Istanbul Zone occurred in an active continental margin-arc setting throughout the Ordovician, transitioning into passive margin conditions following the Silurian transgressive phase. This basin of Gondwanan affinity drifted with the opening of the Paleo-Tethys and completed its tectonic evolution by accreting to Laurussia during the Variscan orogeny (Yilmaz et al. 2025). In the Central Taurides, sedimentological and stratigraphic data indicate that a shallow marine shelf developed along the northern margin of Gondwana during the Middle–Late Devonian, later fragmented by localized volcanism and a rifting phase extending from the Permian into the Triassic, which generated significant subsiding sub-basins (Mackintosh & Robertson 2012).

In a broader Eastern Mediterranean context, microcontinental detachment from Gondwana during the Triassic and the complex evolution of Cimmerian blocks have been invoked to explain successive oceanic openings and closures, including the progressive development of the Neo-Tethys (Robertson & Dixon 1984).

Regional reconstructions from the Black Sea domain further emphasize the long-term interaction between Laurasian crustal blocks and Gondwana-derived terranes, highlighting Paleozoic–Mesozoic subduction, collision, and high-pressure metamorphism associated with Variscan and Cimmerian orogenic processes (Okay & Nikishin 2015). Alternative perspectives on the Early Paleozoic framework of the Eastern Mediterranean propose a Gondwana-derived southern tectonic belt that experienced rifting, passive margin development, and subsequent accretionary processes linked to the evolution of the Paleo-Tethys (Göncüoğlu & Kozlu 2000).

In the Sakarya Zone, Early–Middle Devonian granitoids and Silurian amphibolites document crustal melting and rift-related magmatism along the northern Gondwana margin (Aysal et al. 2012; Topuz et al. 2020). Comparable Early Paleozoic back-arc and arc-related assemblages are preserved in the West Carpathians, where hybrid MORB/OIB-type protoliths and coeval granitoid emplacement reflect immature extensional and accretionary settings prior to Devonian island-arc magmatism and high-pressure metamorphism (Putiš et al. 2009; Vozárová et al. 2022). This Late Paleozoic evolution culminated in mantle-derived alkaline magmatism associated with regional extension and the opening of Triassic oceanic domains (Leitner et al. 2024).

In Anatolide–Tauride Block (ATB), Late Paleozoic successions within the ATB preserve intraplate alkaline volcanism related to extensional tectonics on shallow marine platforms (Robertson et al. 2021). In contrast, mafic volcanic sequences in the Develi–Kayseri region have been interpreted to reflect back-arc basin development within the regional stratigraphic framework (Çimen 2018).

Farther east, Late Devonian to Carboniferous intraplate magmatism in NW Iran and NE Iraq has been attributed to extensional tectonics, mantle plume upwelling, and enriched mantle involvement during the early evolution of the Paleo-Tethyan system (Moghadam et al. 2015; Abdulzahra et al. 2016; Azizi et al. 2017; Mohammadi et al. 2020; Jamei et al. 2021; Veysi et al. 2023). These studies collectively indicate that Late Paleozoic magmatism along the northern Gondwanan margin was not restricted to a single geodynamic regime but instead reflects spatially variable interactions among rifting, back-arc extension, subduction processes, and lithospheric reorganization.

When considered together, these regional and local studies show that the northern Gondwanan margin underwent a long-lasting and spatially heterogeneous tectono-magmatic evolution from the Early Paleozoic to the Triassic. However, despite extensive research on basement evolution and regional plate reconstructions, information on the mantle source characteristics and tectonic significance of Paleozoic metabasic rocks within the ATB remains limited.

Paleozoic metamorphic sequence in the Babadağ (Denizli) region was originally subdivided into two structural levels by Akarsu (1969), who described amphibolites in the lower series characterized by hornblende–albite–titanite–garnet parageneses. Although recent work on Late Devonian amphibolites from the southern Menderes Massif (MM) has documented within-plate mafic magmatism developed under extensional conditions (Koralay 2024), a detailed whole-rock geochemical and isotopic evaluation of the Babadağ metabasic rocks has not yet been undertaken. The present study therefore provides the first comprehensive geochemical characterization of these units, integrating petrography, major and trace elements, REE systematics, and Sr–Nd isotope data. The results offer new constraints on mantle source characteristics, magma evolution, and the Late Paleozoic geodynamic framework of the MM within the ATB.

Geological background

MM constitutes the western part of the ATB of Gondwana affinity (Şengör & Yilmaz 1981; Şengör et al. 1984a). It is bounded to the north and northeast by the Afyon (Candan et al. 2005) and Tavşanlı (Okay 2011) zones, which separate the massif from the İzmir–Ankara–Erzincan Suture Zone (IAESZ) (Şengör & Yilmaz 1981; Okay & Tüysüz 1999; Okay 2008; Göncüoğlu et al. 2010). In the south, the Lycian Nappes are thrust over the massif (Şengör & Yilmaz 1981; Collins & Robertson 1999; Özer et al. 2001; Rimmelé et al. 2003a, b; Bozkurt 2007) (Fig. 1a). The southwestern margin of the MM is delimited by its tectonic relationship with the Cycladic Complex (Ring et al. 1999; Okay 2001).

MM is represented by the Pan-African basement and Paleozoic–Early Tertiary cover series units, which were affected

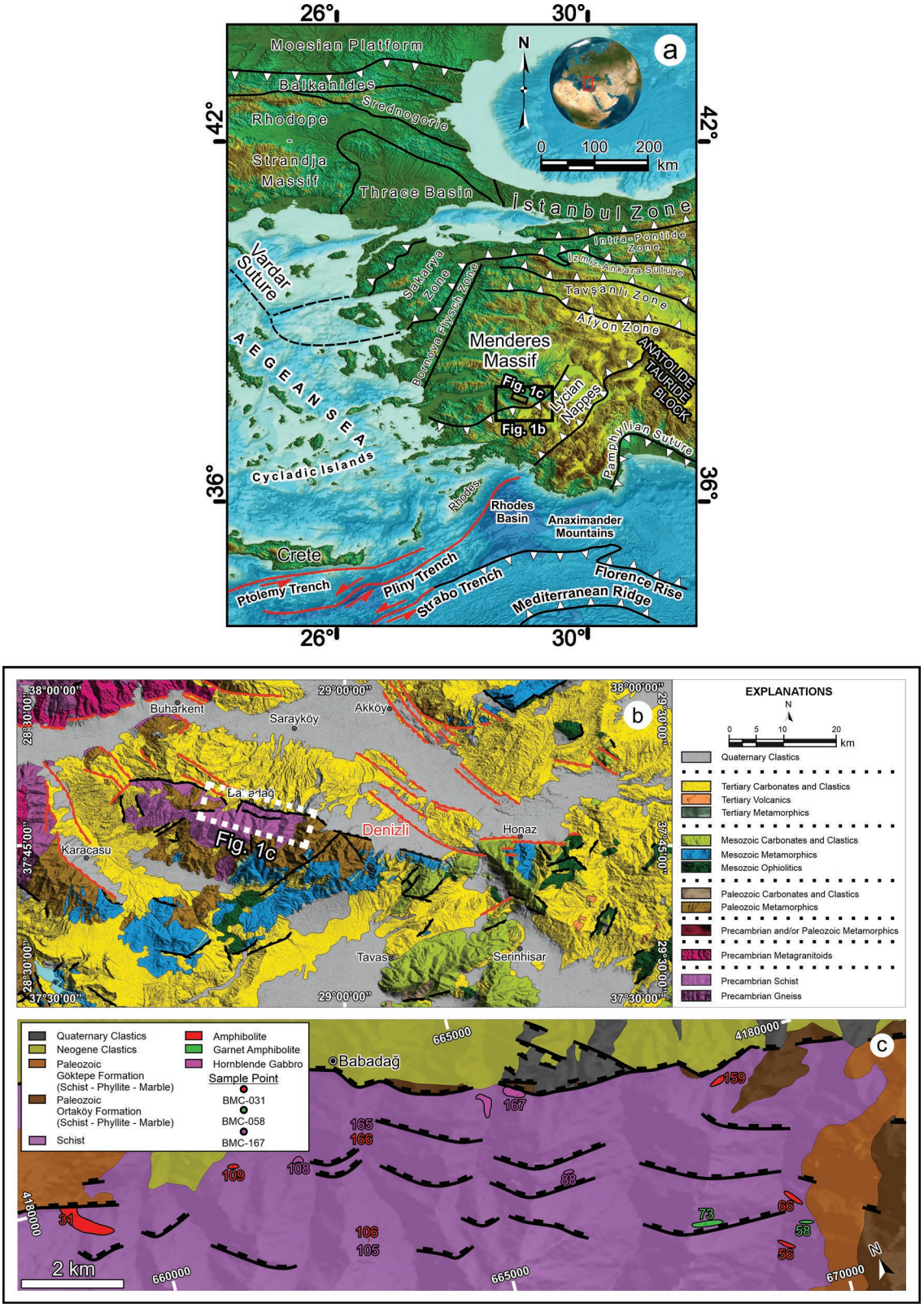

Fig. 1. (a) Western Türkiye, Aegean Sea and Balkans Region. The base elevation data are derived from the Terra Advanced Spaceborne Thermal Emission and Reflection Radiometer (ASTER) Global Digital Elevation Model (GDEM), version 3, with a spatial resolution of approximately 30 m. GEBCO Bathmetry Shaded Relief. Suture zones for Türkiye, Balkans and Aegean Region (Okay & Tüysüz 1999). Morphological structures for Mediterranean basin (Barbot & Weiss 2021). **(b)** 1:500.000 scale geological map Denizli M21–M22 quadrangle (Konak & Şenel 2002). **(c)** The geological map showing the distribution of metabasic rocks in the study area was modified from the 1:25,000 scale M21 quadrangle of The General Directorate of Mineral Research and Exploration.

by polyphase metamorphism (Şengör et al. 1984b; Candan 2011a, b; Dora 2011; Koralay et al. 2011).

The MM preserves a complex geological history linked to the assembly of the Gondwana supercontinent, as evidenced by its Pan-African basement and overlying cover series. The closure of the Mozambique Ocean and the collision of East and West Gondwana during the Late Neoproterozoic–Cambrian period established the foundation for the massif's subsequent tectonic and metamorphic evolution (Candan et al. 2011a). A primary unconformity, reshaped by Alpine compression and extension, is marked by Upper Devonian quartzite–metaconglomerate levels, reflecting the massif's dynamic tectonic regime. The Paleozoic–Early Tertiary cover series, affected by Alpine metamorphism, has been constrained to the Eocene–Oligocene, with medium-pressure Barrow-type metamorphism dominating under greenschist facies conditions (Candan et al. 2011b).

Zircon geochronology (U–Pb, Pb–Pb) from tourmaline and biotite orthogneisses indicates widespread Pan-African acidic magmatism between 590–520 Ma, with crystallization ages of 550–540 Ma (Koralay et al. 2012). Detrital zircons of similar age in Paleozoic schists point to the Pan-African granitoids as source rocks. The Pan-African intrusion age, recorded at 540 Ma for metagabbro protoliths and 530 Ma for eclogite facies metamorphism, aligns with the geodynamic evolution of eclogitic metagabbros derived from acidic protoliths (Oberhänsli et al. 2010). Despite Alpine deformation obscuring direct links to the Mozambique Belt, the MM's tectonic status and geochronology illuminate the final closure of the Mozambique Ocean and the ultimate collision of Gondwana during the Early Cambrian.

Metagabbros of the MM, ranging from Late Neoproterozoic to Early Cambrian, have transformed into eclogitic metagabbro and garnet amphibolites. U–Pb zircon dating supports a crystallization age of 563±1 Ma for the original gabbros, 558±3 Ma for the central eclogitic metagabbro, and 535±3 Ma for the high-pressure overprint, reflecting the timing of magmatic and metamorphic events (Candan et al. 2016). Recent U–Pb data from garnet amphibolite and retrograde eclogite units yield crystallization ages of 537–536 Ma, indicating mafic magmatism during Cadomian extension along the northern Gondwana margin and providing the earliest magmatic records in the massif (Gürsu et al. 2023).

Rapid sedimentation between 570–550 Ma, granite intrusion at 550 Ma, and detrital zircons (900–1100 Ma) linking the MM to Afro-Arabian sources, as well as a major thermal event (260–250 Ma) predating Triassic magmatism, further characterize the massif's evolving crustal architecture (Zlatkin et al. 2013). While the geodynamic and geochronological records of the MM within the ATB are as described, recent research has also provided projections on mantle sources and geotectonic settings for metabasic rocks formed during Late Paleozoic magmatic events. Recent investigations also shed light on mantle sources and geotectonic settings for metabasic rocks, with Devonian amphibolites (367 Ma) in the southern MM evidencing intraplate mafic magmatism in an extensional setting (Koralay 2024).

Analytical methods

During fieldwork in the Babadağ (Denizli) region, fourteen metabasic rock samples were carefully and systematically collected from a range of locations (Supplementary Table S1; Fig. 1c). In the laboratory of the Geological Engineering Department at Pamukkale University, the samples were prepared for analysis. To ensure reliable results, the weathered outer surfaces were trimmed away, and only the fresh, unaltered interiors were selected for further tests. These fresh rock portions were then analyzed for whole-rock major and trace elements, rare earth element (REE) distribution, and Sr–Nd isotope geochemistry (Supplementary Tables S2, S3).

Whole-rock analysis

The rock samples were initially crushed to fragments smaller than 2 mm using a jaw crusher at the Department of Geological Engineering, Pamukkale University. Subsequent grinding was performed in a tungsten carbide mill until at least 85 % of the material passed through a 75 µm sieve. All whole-rock geochemical analyses were conducted at ALS Global Laboratories in Ireland, following comprehensive and standardized analytical procedures. Major oxides, including SiO_2, Al_2O_3, Fe_2O_3, CaO, MgO, Na_2O, K_2O, TiO_2, P_2O_5, MnO, Cr_2O_3, SrO, and BaO, were determined by Inductively Coupled Plasma–Atomic Emission Spectrometry (ICP–AES) after lithium borate fusion, while loss on ignition (LOI) was measured gravimetrically at 1000 °C. Rare earth elements (REE) and other refractory trace elements such as Ba, Ce, Cr, Cs, Dy, Er, Eu, Gd, Hf, Ho, La, Lu, Nb, Nd, Pr, Rb, Sm, Sr, Ta, Tb, Th, Tm, U, V, Y, Yb, and Zr were analyzed by Inductively Coupled Plasma–Mass Spectrometry (ICP–MS) following lithium borate fusion to ensure complete dissolution of resistant mineral phases. Analyses of base metals and transition elements, specifically Ni, Pb, and Sc, were carried out by ICP–AES after near-total digestion using a mixture of four acids: HF, HNO_3, $HClO_4$, and HCl (Supplementary Table S2).

Sr–Nd isotope analysis

Strontium and neodymium isotope geochemistry analyses were carried out at the METU Central Laboratory (R&D Training and Measurement Centre, Radiogenic Isotope Laboratory) based on the procedures described by Köksal (2019) and following the laboratory's established experimental protocols. Weighing, chemical dissolution, and chromatography were performed under Class 100 clean lab conditions, using ultrapure water and reagents. For strontium and neodymium analyses, approximately 80 milligrams of sample were weighed and placed into PFA vials. The samples were fully dissolved in

4 ml of 52 % HF for four days at temperatures above 100 °C on a heating plate. After near-complete evaporation, the residues were redissolved in 4 ml of 6 N HCl on the heating plate for one day. Following another drying step close to evaporation, the samples were dissolved in 1 ml of 2.5 N HCl to prepare for chromatography. Strontium was separated using Bio Rad AG50 W–X8 (100–200 mesh) resin in 2 ml Teflon columns with 2.5 N HCl. After isolating strontium, the rare earth element fraction was collected with 6 N HCl. Strontium was loaded onto a single Re filament using Ta activator and 0.005 N H_3PO_4, and measured in static mode. $^{87}Sr/^{86}Sr$ data were normalized to $^{86}Sr/^{88}Sr=0.1194$. During the analyses, Sr was measured as the NBS 987 standard at 0.710265±12 (n=3). Neodymium was separated from other rare earth elements in 2 ml Teflon columns using HDEHP–coated biobeads (Bio Rad resin) and 0.22 N HCl. The isolated neodymium was loaded with 0.005 N H_3PO_4 onto the Re filament and measured in static mode using the double filament technique. $^{143}Nd/^{144}Nd$ data were normalized to $^{146}Nd/^{144}Nd=0.7219$. The LaJolla standard for Nd was measured at 0.511850±5 (n=2). No bias correction was applied to the strontium and neodymium isotope ratio measurements. Isotope ratio determinations were performed by multiple collection using a Triton Thermal Ionisation Mass Spectrometer (Thermo–Fisher). Analytical uncertainties are reported at the 2 sigma level (Supplementary Table S3).

Results

Field relations and petrography of metabasic rocks

The core series comprises layers and bands of mica schist, garnet schist, muscovite schist, garnet–albite–mica schist, and black quartz–muscovite schist. Metabasic rocks, characteristic of the core series, are occasionally found as bands within the schist units, and are also present as sills and stocks where their primary igneous features are preserved. Hornblende gabbros display minimal evidence of magmatic deformation, whereas amphibolite and garnet amphibolite typically exhibit foliation and syn-tectonic structures, along with cleavages that intersect the foliation. Schistosity is especially well-developed in amphibolite and garnet amphibolite. In some localities, amphibolites are observed in direct contact with marble, and inclusions of marble are found within the amphibolite.

An unconformity, characterized by transitional meta-conglomerate units, separates the core series from the overlying cover series. The cover sequence consists of garnet phyllite, chloritoid phyllite, muscovite schist, and marble (Fig. 1c).

Metabasic rocks distributed across the study area have been grouped into three petrographic categories. Based on similarities in their mineral assemblages, they are classified as amphibolite, garnet amphibolite, and hornblende gabbro (Fig. 2). Retrograde metamorphic features are generally observed in all metabasic rocks, and evidence of low-temperature transformation related to hydrothermal alteration is present. Due to this alteration, hornblende gabbro units in some outcrops are found as metagabbro (Fig. 2).

Amphibolite

Amphibolite typically displays a nematoblastic texture, while in those units where plagioclase minerals are relatively larger and equant, a nemato-porphyroblastic texture is observed. The principal minerals are amphibole, albite, zoisite, chlorite, quartz, and minor amounts of garnet. Amphibole crystals are elongated and rod-shaped, and in some instances, they are partially replaced by epidote. Albite commonly occurs as porphyroblasts, with polysynthetic twinning present in certain grains. Zoisite exhibits high relief and often appears as inclusions within albite. Chlorite is pale green and is seen replacing garnet, which is only rarely present. Titanite is present and has partially altered to leucoxene, forming fine-grained, dull, and generally opaque aggregates of titanium dioxide. Amphibolite shows evidence of hydrothermal alteration and retrograde metamorphism at low temperatures, as indicated by the replacement of garnet by chlorite and titanite, the formation of leucoxene, and the occurrence of zoisite (Fig. 3a–a').

Garnet amphibolite

Garnet amphibolite displays a porphyroblastic texture, reflecting the presence of both albite and relatively large garnet crystals. The primary minerals are amphibole, albite, garnet, chlorite, biotite, and quartz. Amphibole crystals are elongated and rod-shaped. While garnet is present to some degree in other metabasic rocks, in garnet amphibolite it forms larger porphyroblasts (~2–3 mm in size), especially in zones affected by chloritization. Garnet commonly exhibits microtectonic features, including syn-tectonic snowball structures (Fig. 3b). Biotite is relatively rare but is frequently altered to chlorite (Fig. 3b–b').

Hornblende gabbro

Hornblende gabbro has a relatively well-preserved magmatic texture compared to other metabasic rocks and exhibits a phenocrystalline composition in terms of plagioclase and hornblende. The main minerals are amphibole, plagioclase, garnet, chlorite, biotite, epidote, quartz, and muscovite. Amphibole minerals retain its original euhedral shapes when it occurs as phenocrysts in igneous rock and exhibits distinct cleavage planes. Plagioclase minerals exhibit polysynthetic twinning. In some locations, garnet minerals are observed in hornblende gabbro content and are easily identified by their high relief characteristics in parallel nicol. Local epidotization of amphibole minerals is observed. Biotite minerals are present in small amounts. In locations where the garnet content is relatively higher, the hornblende gabbro unit exhibits a metagabbroic appearance. Metagabbroic rocks exhibit retrograde metamorphic features characterized by the replacement of garnet

Fig. 2. Metabasic rocks outcrops around Babadağ (Denizli) region. **(a)** Cleavage planes (yellow dashed line) intersecting foliation planes in amphibolite (BMC–031). **(b)** Stock-like exposure of amphibolite displaying a massive (BMC–159). **(c)** Contact relationship between garnet amphibolite and schist (BMC–058). **(d)** The sill-shaped settlement of hornblende gabbro (BMC–105). **(e)** Hornblende gabbro outcrop exhibiting a massive, blocky structure with multi-directional jointing (BMC–108). **(f)** Field view of the altered hornblende gabbro stock (BMC–167).

by biotite and chlorite. Muscovite minerals are observed in units close to schists in the field. Titanite has partially altered to leucoxene (Fig. 3c–c').

Whole-rock geochemistry

Rock classification

Geochemical discrimination diagrams were utilized to determine both the protolith characteristics and tectonic setting of the metabasic rocks. On the TiO_2 (wt.%) vs Ni (ppm) diagram (Fig. 4a), all samples fall within the ortho-amphibolite field, which is indicative of an igneous origin (Leake 1964). To minimize the influence of metamorphic alterations, ratios of immobile elements were evaluated. The Nb/Y vs Zr/Ti plot (Fig. 4b) shows that the metabasic rocks possess transitional to alkaline affinities, with most data points clustering in the alkali basalt region (Pearce 1996). Similarly, the Nb/Y vs Zr/P_2O_5 diagram (Fig. 4c) reveals that the samples are distributed between alkaline and tholeiitic basalt fields (Floyd & Winchester 1975). This dual character implies that the precursor magmas were derived from varying degrees of partial melting in the mantle, suggesting a complex petrogenetic history rather than a single, uniform magma series.

Major oxides and trace elements composition

The whole-rock geochemical data for the metabasic rocks are summarized in Supplementary Table S2. In the CaO/Al_2O_3 vs MgO diagram, a clear pattern emerges indicating that clinopyroxene (Cpx) fractionation plays a dominant role in

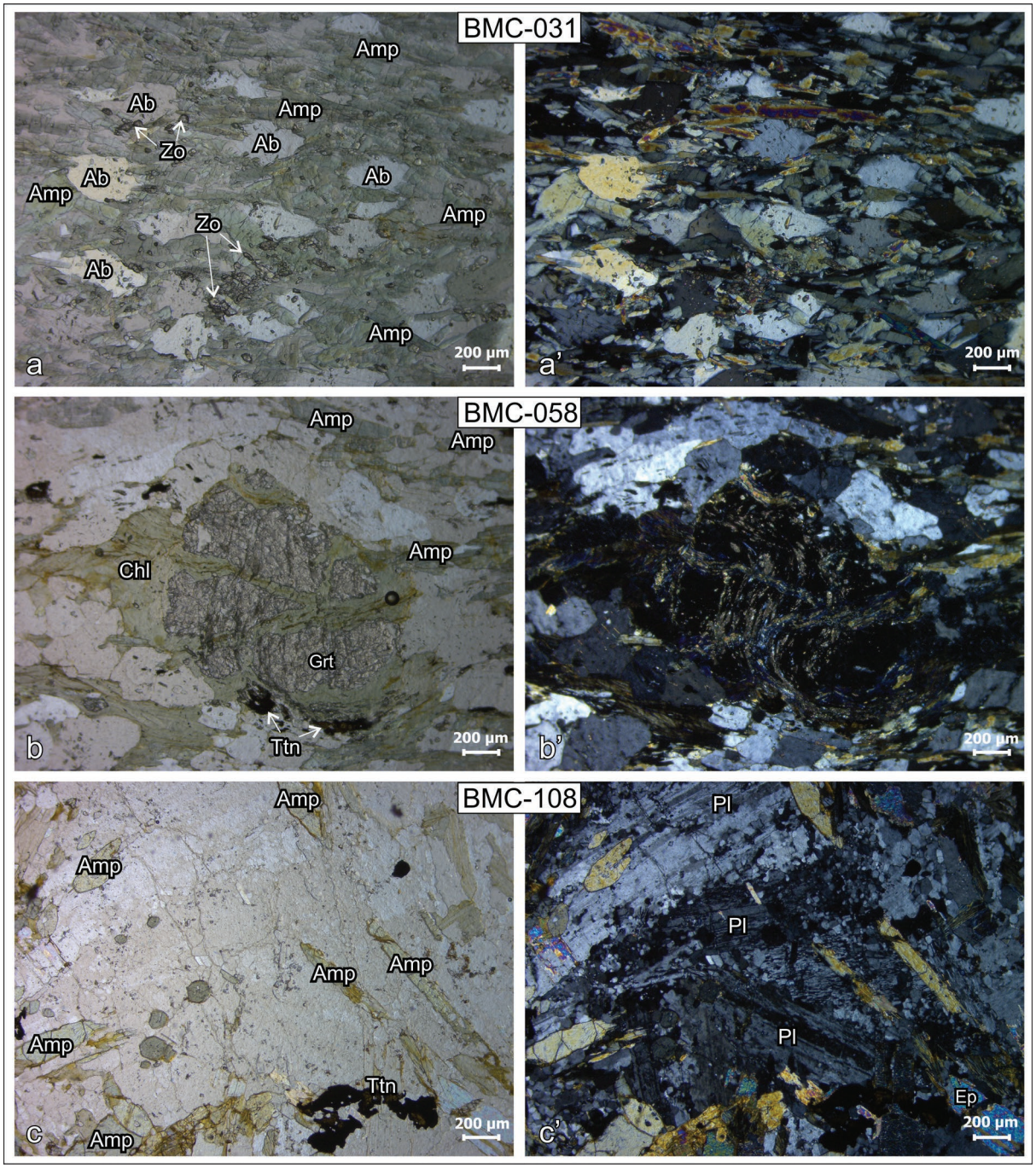

Fig. 3. Microphotographic images of metabasic rocks: amphibolite (a – parallel nicol, a' – cross nicol); garnet amphibolite (b – parallel nicol, b' – cross nicol); hornblende gabbro (c – parallel nicol, c' – cross nicol). Ab: Albite; Zo: Zoisite; Chl: Chlorite; Amp: Amphibole; Grt: Garnet; Pl: Plagioclase; Ttn: Titanite; Ep: Epidote. Mineral abbreviations are taken from Whitney & Evans (2010).

the petrogenesis of these rocks. The systematic decline in the CaO/Al_2O_3 ratio with decreasing MgO demonstrates the preferential removal of CaO from the melt as clinopyroxene crystallizes. The close alignment of data points along the clinopyroxene (Cpx) vector further supports this mineralogical control. This trend suggests that the various lithological units are cogenetic and represent a sequence of magmatic differentiation stages from a common parent magma.

In the TiO_2 vs MgO plot, there is a distinct negative correlation, with TiO_2 content increasing as MgO decreases. This relationship reflects the incompatible behavior of titanium during the early to intermediate phases of magmatic evolution, indicating that Ti-bearing oxides such as ilmenite and titanomagnetite did not play a significant role in fractionation. The progressive enrichment of TiO_2 in the residual melt is

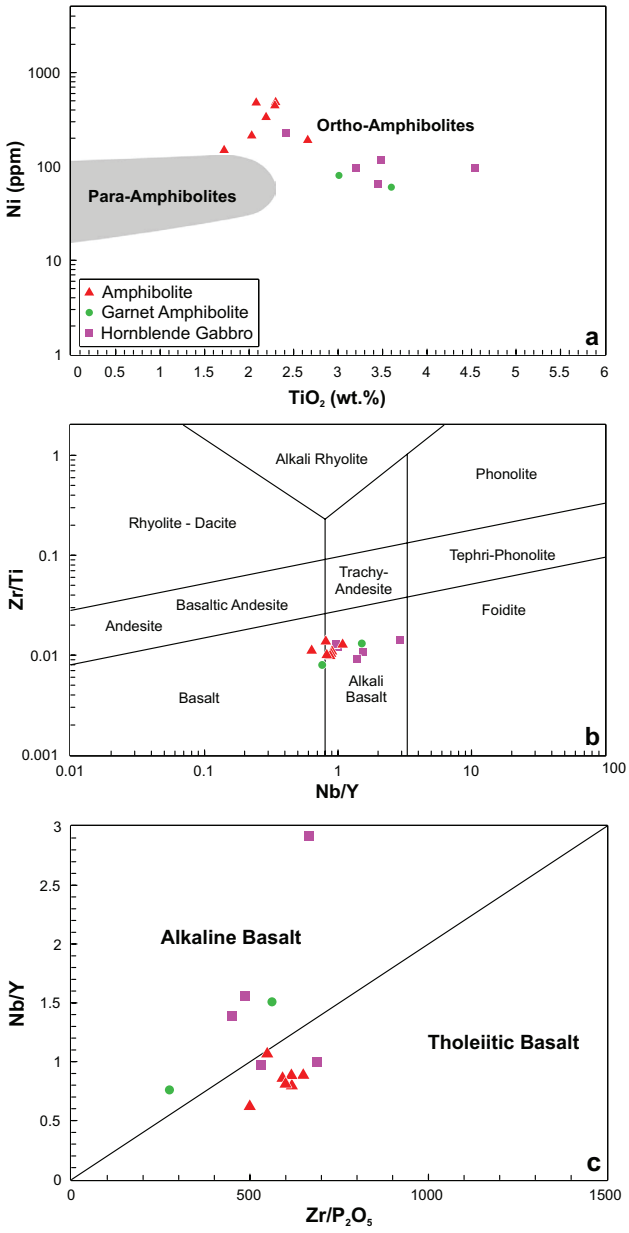

Fig. 4. Classification diagrams of metabasic rocks. **(a)** Ni vs TiO_2 (Leake 1964); **(b)** Zr/Ti vs Nb/Y (Pearce 1996); **(c)** Nb/Y vs Zr/P_20_5 (Floyd & Winchester 1975).

consistent with the transitional to alkaline character of the precursor magmas.

The Ni and Cr vs MgO diagrams reveal strong positive correlations, marked by a pronounced drop in Ni and Cr concentrations as MgO decreases. This pattern points to the highly compatible nature of nickel and chromium, signifying the early removal of olivine and spinel. Elevated Ni and Cr at higher MgO values indicate that the source magmas were relatively primitive and underwent substantial extraction of mafic minerals early in their evolution. The apparent gap in Cr concentrations at intermediate MgO levels (~10–12 wt.%) may be attributed either to the rapid extraction of spinel from the melt or to sampling limitations. However, the continuous trend in Ni, with a single sample present in this range, suggests steady differentiation rather than a major compositional gap.

The distributions of Sc, Y, Zr, and Th vs MgO (6.07–14.85 wt.%) provide valuable insight into the magmatic evolution and mineral control within the suite. Incompatible elements such as Y, Zr, and Th display well-defined negative correlations with MgO, reflecting their progressive enrichment in the residual melt during fractional crystallization and confirming the cogenetic relationship among samples. The enrichment of high field strength elements (Y, Zr) and Th is typical of a transitional magmatic affinity. In contrast, the relatively flat or slightly decreasing trend of Sc, compared to other trace elements, offers quantitative evidence for clinopyroxene fractionation, as Sc is preferentially incorporated into clinopyroxene during the evolution from primitive to more evolved magmatic compositions (Fig. 5).

Multi-element variation

The primitive mantle-normalized multi-element patterns (Fig. 6a) display marked enrichment relative to N-MORB, with profiles falling between those of E-MORB and OIB, and showing a predominant affinity for an OIB-like signature. Although the mobility of Cs, Rb, and Ba during metamorphism can complicate interpretations, the pronounced sodic character of the rocks, as evidenced by high Na_2O contents (1.36–4.65 wt.%) and notably low K_2O (0.07–1.34 wt.%), corresponds well with the strong negative K anomaly seen in the spider diagrams. This systematic potassium depletion is interpreted as a primary magmatic feature, which may reflect the influence of K-bearing residual phases in the source region, rather than being an artifact of metamorphic leaching (Fig. 6a).

A distinctive aspect of the trace element patterns is the decoupling of Nb and Ta. While Nb displays a relative negative anomaly, its geochemical analogue Ta does not show similar depletion and instead follows the OIB reference trend. Titanium concentrations are also elevated, in line with OIB-like enrichment. In contrast to subduction-related settings, which typically exhibit coupled depletion in high field strength elements (Nb, Ta, Ti), the enrichment of Ta and Ti in these samples supports an intra-plate magmatic origin rather than an arc-related one. The relative depletion in Nb alone may indicate the involvement of continental crustal components or inheritance from a subduction-modified lithospheric mantle, as suggested by pronounced Pb, Th, and U peaks (Fig. 6a).

In terms of crystallization history, the consistent Sr depletion combined with the observed CaO contents (6.44–10.45 wt.%) confirms the role of plagioclase fractionation. The absence of, or only slightly negative, Eu anomalies suggest that plagioclase fractionation played a subordinate role during magma evolution, potentially due to high water content or elevated oxygen fugacity suppressing plagioclase stability.

The rare earth element (REE) patterns show a slight decline from Gd to Lu, producing a near-flat HREE profile. This trend

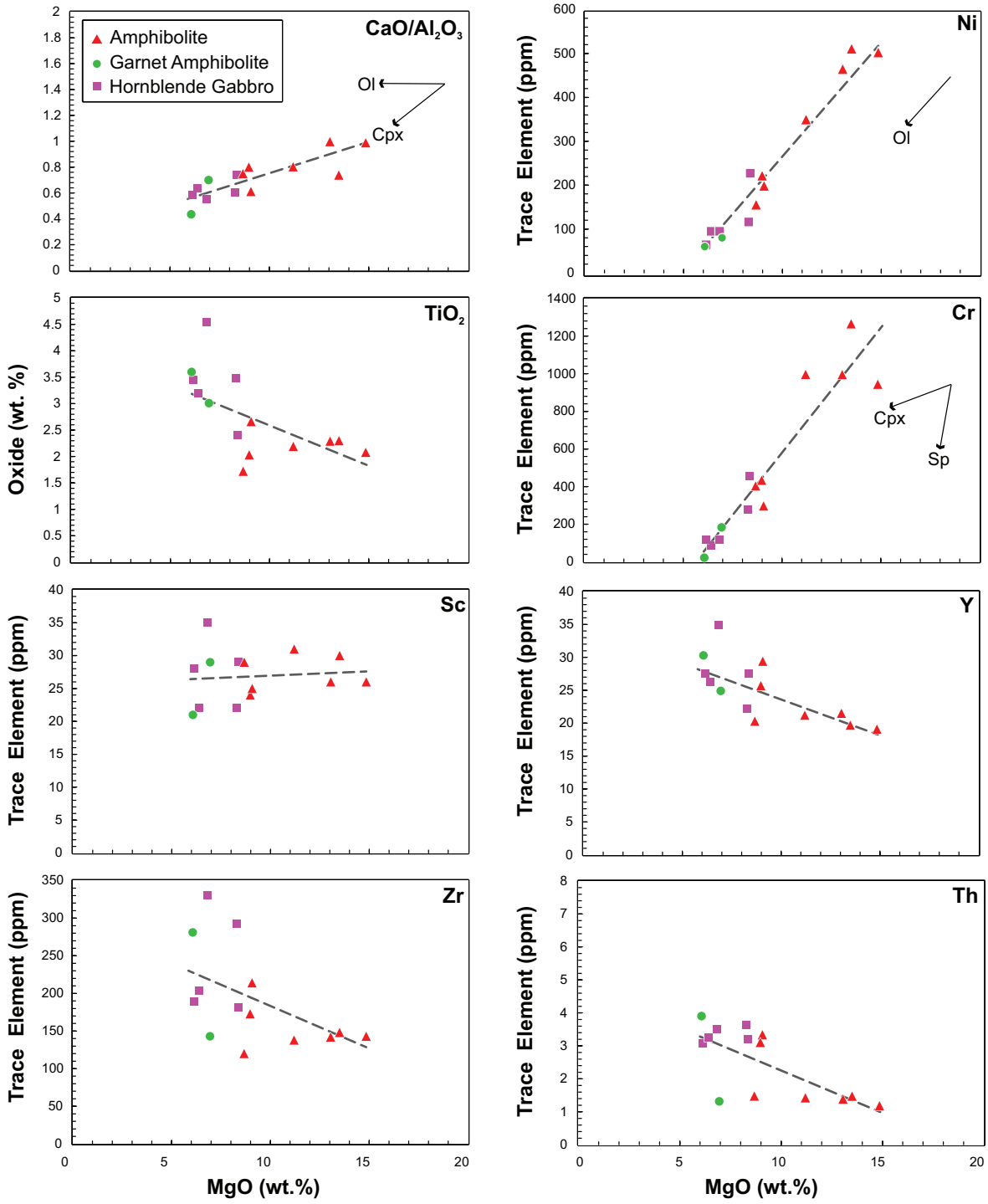

Fig. 5. Distribution of the major oxide (Ca_2O/Al_2O_3 and TiO_2 by weight %) and trace elements (Ni, Cr, Sc, Y, Zr, Th in ppm) in metabasic rocks versus MgO, and theirs linear regression trend – fractional crystallization – (gray dashed line). Ol: Olivine; Cpx: Clinopyroxene; Spl: Spinel. Mineral abbreviations are taken from Whitney & Evans (2010).

indicates a minimal role for residual garnet in the source, suggesting that melting occurred in the spinel–garnet transition zone rather than at greater depths. While these geochemical features provide a robust qualitative framework, further validation through quantitative petrogenetic modeling is warranted (Fig. 6a).

Discussion

Mantle source characteristics

On the chondrite-normalized REE diagram, amphibolite samples are tightly clustered and follow sub-parallel trends,

reflecting their homogeneous character and a shared magmatic lineage. The significant enrichment in light rare earth elements (LREEs) relative to heavy rare earth elements (HREEs) points to a source from enriched mantle with an OIB-like signature, rather than a depleted N-MORB or moderately enriched E-MORB source. The nearly flat HREE trend, with a slight decrease from Gd to Lu, indicates that partial melting occurred at moderate depths within the spinel–garnet transition zone, where residual garnet had little influence on melt composition. Additionally, the absence of a pronounced negative Eu anomaly suggests that plagioclase fractionation was not the dominant process, or that it was balanced by plagioclase accumulation during magmatic evolution (Fig. 6b).

When plotted on the Sr–Nd isotopic diagram, the samples fall within or near the enriched mantle array defined by global mantle reservoirs (Zindler & Hart 1986) (Supplementary Table S3) (Fig. 7). The relatively restricted Nd isotopic variation compared to the broader Sr range suggests that Nd largely preserves mantle source characteristics, whereas Sr isotopes may reflect secondary modification. In addition, Mg# values (~45–70) indicate variable degrees of magmatic differentiation, consistent with fractional crystallization during magma evolution (Supplementary Table S2).

The Nb/La versus La/Yb diagram provides additional constraints on mantle source characteristics. Most samples plot within or close to the asthenospheric mantle field and cluster around average OIB compositions, whereas several samples occupy a transitional position between asthenospheric and lithospheric mantle domains (Fig. 8). Their separation from the lower crust field indicates that crustal assimilation was not the primary control on Nb/La systematics, although minor contributions cannot be entirely excluded. Garnet amphibolite samples display relatively higher La/Yb values, consistent with slightly deeper melting conditions within the spinel–garnet transition regime. Overall, the diagram indicates an enriched mantle source dominated by an asthenospheric signature with subordinate lithospheric contribution.

The metabasic rocks investigated in this study exhibit geochemical characteristics consistent with derivation from an enriched mantle source. Zr/Nb ratios (4.5–9.5) and La/Nb values (0.52–1.02) fall within the range commonly attributed to OIB-like to transitional enriched mantle compositions and contrast with depleted MORB-type sources, consistent with enriched mantle reservoirs characterized by elevated incompatible element abundances (Pearce 1983; Hofmann 1988; Sun & McDonough 1989). Elevated Ti contents (~10,000–27,000 ppm) and chondrite-normalized $(La/Yb)_{cn}$ values of 5–16 indicate LREE-enriched mantle signatures and variable degrees of partial melting of an enriched source domain rather than melting of a strongly depleted mantle reservoir (Supplementary Table S2).

MREE–HREE systematics, including elevated Sm/Yb ratios together with chondrite-normalized $(Dy/Yb)_{cn}$ values

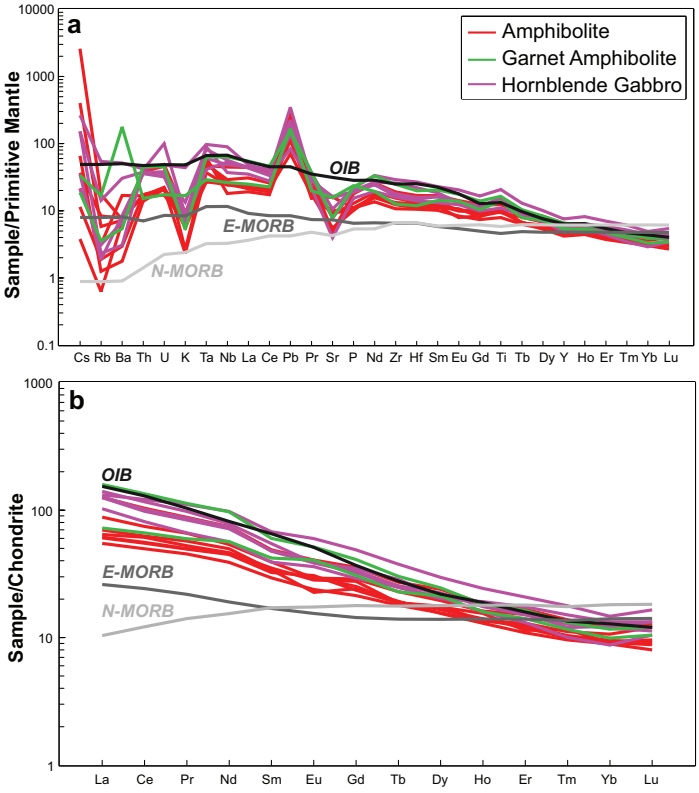

Fig. 6. (a) Multi–element variation patterns normalised relative to the primary mantle. **(b)** REE patterns normalised relative to chondrite (Sun & McDonough 1989).

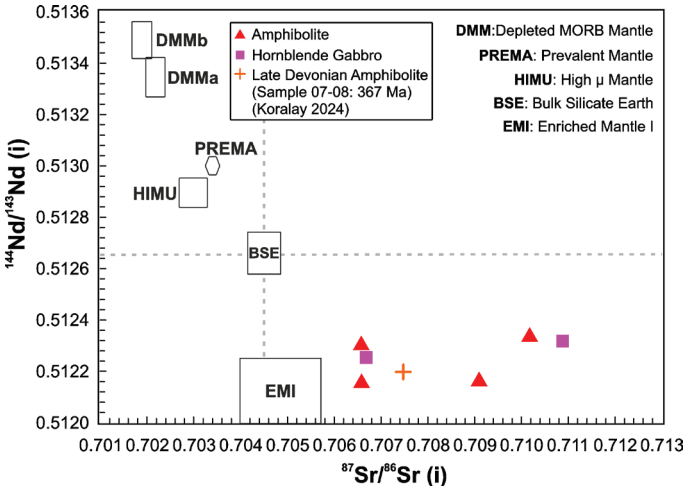

Fig. 7. The isotope ratio between $^{144}Nd/^{143}Nd$ (i) and $^{87}Sr/^{86}Sr$ (i) (Zindler & Hart 1986) for metabasic rocks. The isotope ratio of the Late Devonian (367 Ma) amphibolite belonging to the metabasic rock of the southern Menderes Massif in Koralay (2024). The $^{144}Nd/^{143}Nd$ (i) and $^{87}Sr/^{86}Sr$ (i) plot was prepared using PetroGram Excel© based on Gündüz & Asan (2021).

commonly exceeding 1.5, are consistent with melting near the spinel–garnet transition zone, where residual garnet begins to influence MREE–HREE fractionation (Wilson 1989; Rollinson 1993). These values do not require melting exclusively within the garnet stability field but indicate a transitional depth regime between spinel- and garnet-bearing peridotite sources. Nb/Ta ratios range from sub-primitive to near-primitive mantle values, suggesting that HFSE systematics were broadly preserved during magma generation, although some variability reflects source heterogeneity. Nb/U ratios (16–63) span from sub-primitive to primitive mantle values (PM: ~47), indicating that most samples retain mantle-like Nb–U characteristics (Hofmann et al. 1986) (Fig. 9).

Although these geochemical features collectively indicate an enriched mantle reservoir, Ce/Pb ratios (2–10) are significantly lower than typical MORB–OIB values (~20–30; Hofmann et al. 1986), indicating relative Pb enrichment (Fig. 9). The coexistence of largely mantle-like Nb/U values with markedly low Ce/Pb ratios suggests that the mantle source was compositionally heterogeneous and may have experienced prior metasomatic modification, either through subduction-related processes or limited crustal interaction.

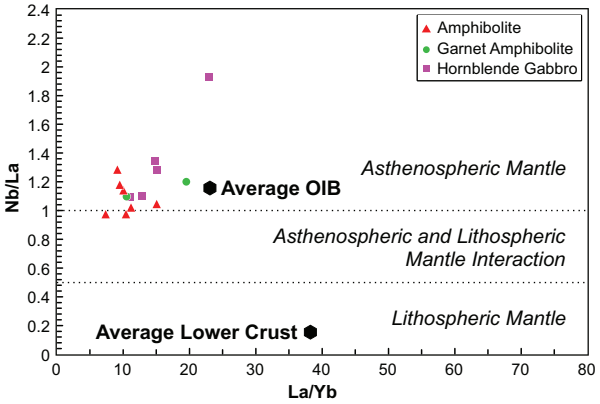

Fig. 8. Diagram to discriminate between the asthenosphere and lithosphere mantle. Nb/La vs La/Yb diagram was used based on information obtained from Abdel-Rahman (2002). Average OIB is after Fitton et al. (1991); Average Lower Crust (average of six lower crustal granulite xenoliths is represented here) is after Chen & Arculus (1995). The dashed lines separating the asthenosphere, lithosphere and their interaction mantle zones are plotted based on the data provided by Smith et al. (1999).

Within a broader regional framework extending from the western Carpathians through the ATB to NW Iran and the Iraq segment of the northern Gondwanan (Paleo-Tethyan) margin, Late Paleozoic magmatic systems display variable but commonly enriched mantle contributions during extensional phases.

Western Carpathians meta-igneous rocks show geochemical features ranging from MORB-like to enriched affinities (Putiš et al. 2009). The Zemplinic Unit similarly exhibit transitional MORB–OIB characteristics, indicating a heterogeneous mantle source rather than a uniformly depleted reservoir (Vozárová et al. 2022).

These transitional signatures are compatible with melting regimes involving variable asthenospheric input. Permian synsedimentary volcanism in the eastern Alps records enriched mantle signatures with preserved HFSE systematics, attributed to asthenospheric involvement during lithospheric thinning (Leitner et al. 2024). Although temporally younger, these data demonstrate that enriched mantle domains were active along the same margin during post-orogenic extension.

Within the ATB, Late Devonian amphibolites of the southern MM display enriched mantle affinities within a within-plate extensional framework (Koralay 2024). Late Paleozoic volcanic rocks from the Binboğa unit likewise indicate enriched mantle derivation during extensional tectonics, albeit with minor subduction inheritance (Robertson et al. 2021). In contrast, mafic volcanics from the eastern Taurides show clearer back-arc and subduction-related geochemical traits (Çimen 2018), illustrating lateral mantle variability within the same tectonic belt.

In NW Iran, Late Devonian–Carboniferous A-type granitoids and associated mafic rocks reflect enriched and compositionally heterogeneous mantle sources activated during intracontinental extension. Azizi et al. (2017) describe this

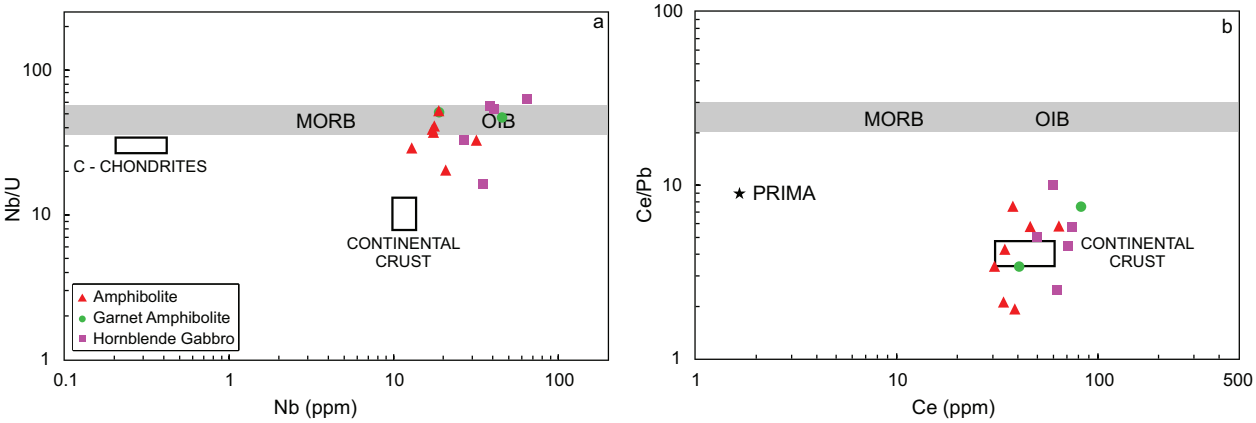

Fig. 9. Diagrams show the concentrations of Nb/U vs U **(a)** and Ce/Pb vs Pb **(b)** in the primitive mantle (PRIMA), chondrite, MORB, OIB, and continental crust (Hofmann et al. 1986).

magmatism as derived from an enriched source involving asthenospheric upwelling, while Mohammadi et al. (2020) emphasize mantle enrichment rather than derivation from a depleted MORB-type reservoir. Moghadam et al. (2015) interpret the bimodal magmatism as a product of enriched mantle input, indicating a chemically non-uniform reservoir. Regarding the Iraq segment, Devonian A-type granites are interpreted as mantle-derived magmatic products linked to the same extensional regime (Abdulzahra et al. 2016). Collectively, these studies highlight asthenospheric contributions beneath a thinned lithosphere.

This evidence supports the existence of compositionally heterogeneous mantle domains rather than a single uniform reservoir beneath the northern Gondwanan margin.

Taken together, the geochemical and isotopic data presented here, in comparison with regional studies from the Western Carpathians through the ATB to NW Iran and the Iraq segment of the northern Gondwanan (Paleo-Tethyan) margin, indicate that Paleozoic magmatism along this margin involved variable contributions from enriched asthenospheric mantle, locally modified lithosphere, and inherited subduction components. In this context, the enriched trace-element patterns, transitional spinel–garnet melting signatures, mantle-like Nb/U ratios, and low Ce/Pb values documented in the present study are best explained by melting of a compositionally heterogeneous mantle domain during extensional tectonic conditions, rather than derivation from a depleted MORB-type reservoir.

Evidence for mantle source modification

The limited variation in Nd relative to the broader range in Sr indicates that Nd isotopes largely preserve primary mantle source characteristics, whereas Sr isotopes are more susceptible to modification due to their greater mobility in fluid-related processes.

Systematic relationships between isotopic and trace-element parameters provide internally consistent evidence for source modification. The inverse relationship between $^{87}Sr/^{86}Sr$ and Ce/Pb, together with the association of more radiogenic Sr values with comparatively lower Nb/U and moderately elevated Th/Nb ratios, indicates that isotopic enrichment and trace-element systematics are coherently linked rather than reflecting independent secondary processes.

Ce/Pb ratios (1.9–7.6) are markedly lower than the canonical mantle value (~25±5), indicating the involvement of a Pb-enriched component (Hofmann et al. 1986) (Fig 9). Such Pb enrichment is commonly associated with mantle heterogeneity and the incorporation of incompatible element-rich components within enriched mantle domains (Hofmann 1997). The wide range of Nb/U ratios (16–63), evaluated relative to the characteristic mantle range defined by Hofmann et al. (1986), further indicates source heterogeneity rather than derivation from a chemically uniform asthenospheric reservoir (Fig. 9). Moderately elevated Th/Nb and Th/Ta ratios relative to MORB values, yet remaining below typical arc thresholds (Pearce 2008), additionally suggest enrichment by incompatible element-rich components without requiring a typical subduction-related magmatic setting. Notably, whereas Nb-based systematics plot largely within or close to OIB-like mantle fields, Ce/Pb ratios cluster within the continental crustal range, highlighting a decoupling between HFSE behavior and fluid-mobile element signatures.

If the low Ce/Pb ratios resulted from crustal assimilation during magma ascent, Nb/U values would commonly be expected to shift toward crustal compositions and isotopic mixing trends would be observed. However, the decoupling between Ce/Pb and Nb/U does not support significant assimilation fractional crystallization (AFC) processes and instead supports source-level chemical modification.

The geochemical decoupling between mantle-like Nb systematics and crustal-range Ce/Pb ratios observed in this study is not unique within the Late Paleozoic evolution of the northern Gondwanan margin. Comparable indications of mantle heterogeneity and source modification have been reported from the western Carpathians through the ATB to NW Iran and the Iraq segment of the northern Gondwanan (Paleo-Tethyan) margin, although the processes invoked vary regionally.

Western Carpathian magmatism reflects mantle domains influenced by supra-subduction processes and subsequent tectonic reactivation (Putiš et al. 2009). These signatures are attributed to metasomatic enrichment that altered the original mantle source composition (Vozárová et al. 2022).

Permian volcanism in the Eastern Alps records enriched mantle signatures variably affected by metasomatic overprinting and open-system processes during post-orogenic extension (Leitner et al. 2024).

Within the ATB, Late Devonian mafic magmatism in the southern MM has been discussed in terms of enrichment processes involving assimilation and fractional crystallization (Koralay 2024), whereas volcanic units from the Binboğa region display enriched signatures with limited subduction inheritance (Robertson et al. 2021). In contrast, mafic volcanics from the Eastern Taurides show clearer back-arc and subduction-related characteristics (Çimen 2018), emphasizing spatial variability in mantle modification within the same tectonic belt.

Petrogenetic indicators in NW Iran and Iraq provide significant evidence for a modified mantle source. In NW Iran, Mohammadi et al. (2020) highlight mantle heterogeneity combined with magma mixing and limited crustal interaction, while Moghadam et al. (2015) note that enriched mantle input was accompanied by assimilation and fractional crystallization (AFC). Similarly, Jamei et al. (2021) attribute the magmatism to parental magmas that evolved through fractional crystallization and limited crustal interaction. In the Iraq segment, mantle-derived magmatic products also show signs of possible minor crustal interaction (Abdulzahra et al. 2016). Furthermore, Central Iranian lamprophyres display isotopic and trace element characteristics consistent with a metasomatized lithospheric mantle source influenced by earlier subduction processes (Veysi et al. 2023).

Collectively, the regional evidence indicates that Paleozoic mantle domains along this margin were variably enriched and chemically heterogeneous, reflecting differing degrees of metasomatism and limited crustal interaction rather than derivation from a uniformly depleted reservoir. In this framework, the low Ce/Pb ratios coupled with largely mantle-like Nb/U values documented in the present study are most consistently explained by source-level chemical modification within an enriched mantle domain during extensional tectonic conditions.

Geotectonic settings

Multiple tectonic discrimination diagrams consistently indicate that the metabasic rocks of the southern MM formed in an extensional intraplate geodynamic setting. On the Ti/Y versus Nb/Y diagram, the samples plot within the sub-alkaline to alkaline within-plate basalt field, indicating magmatism associated with lithospheric extension rather than a dominantly subduction-related process (Pearce 1982) (Fig. 10a). This interpretation is further supported by the La/10–Y/15–Nb/8 ternary diagram, where the samples fall within continental and alkaline basalt fields characteristic of anorogenic magmatism typically developed in extensional intracontinental domains (Cabanis & Lecolle 1989) (Fig. 10b). The distribution of samples within late- to post-orogenic and anorogenic distensive domains further supports magma generation in a continental extensional regime.

Additional constraints are provided by Ti/V systematics, with values ranging from 43 to 70, placing most samples within the OIB-alkaline field and the remainder overlapping the upper MORB range (Ti/V=36.85–64.34), indicating a high-Ti mantle source consistent with deep–seated melting in an intraplate environment (Shervais 2022) (Fig. 10c). Similarly, the Th–Nb normalized diagram shows enrichment trends typical of OIB-like magmatism evolving from MORB-like compositions toward alkaline basalts under rifting conditions (Saccani 2015) (Fig. 10d). These geochemical characteristics collectively do not support a dominant subduction-related magmatic regime and instead indicate melt generation in a within-plate extensional setting.

In continental rift environments, magma generation is commonly associated with lithospheric thinning and thermally

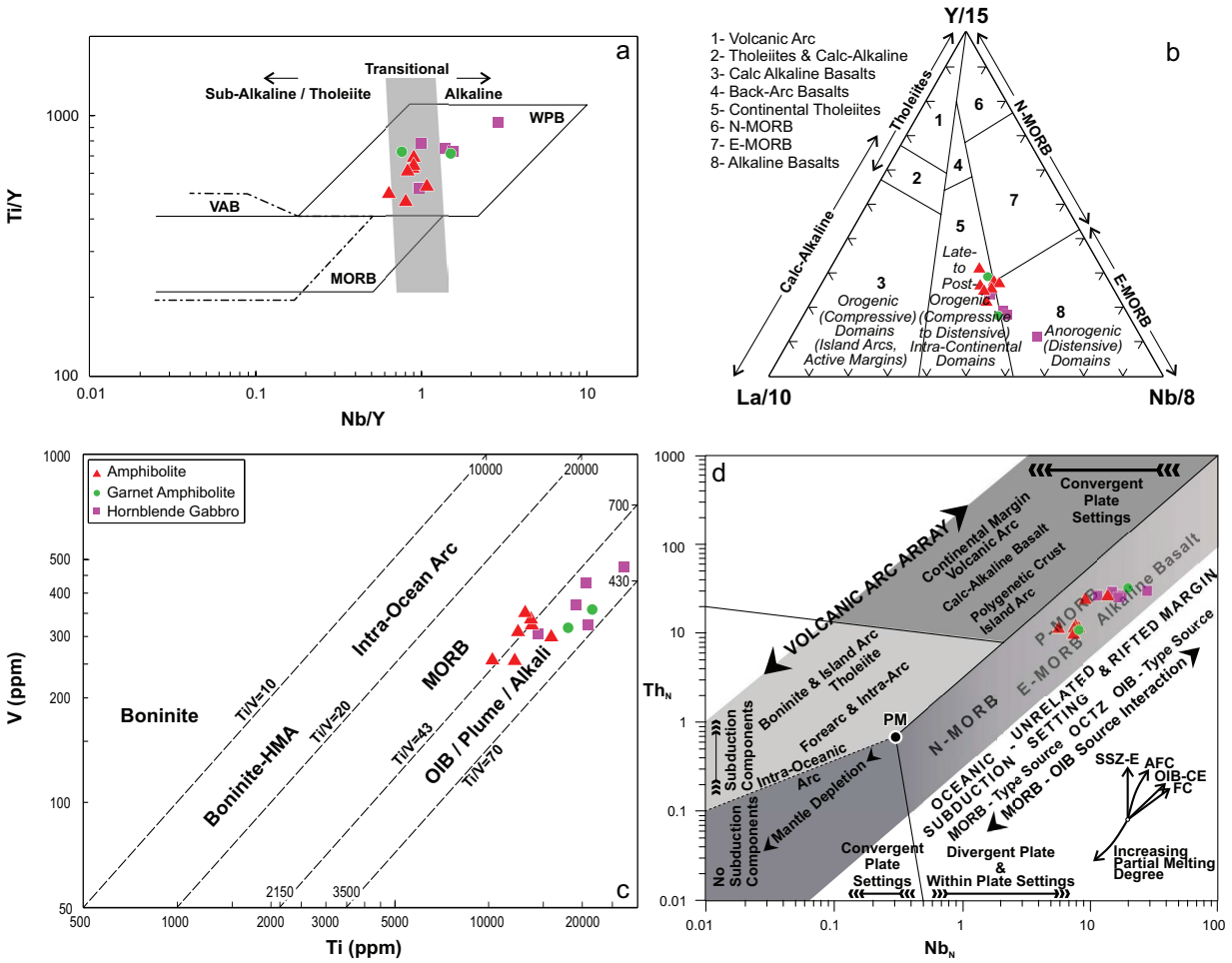

Fig. 10. Geotectonic environment discrimination diagrams. **(a)** Ti/Y vs Nb/Y (Pearce 1982), **(b)** La/10 – Y/15 – Nb/8 ternary diagram (Cabanis & Lecolle 1989), **(c)** V vs Ti (Shervais 2022), **(d)** Th_N vs Nb_N diagram (Saccani 2015) plot was prepared using Geochemical Data Toolkit (GCDkit) based on Janoušek et al. 2006.

driven asthenospheric upwelling, which promotes decompression melting of mantle material (McKenzie & Bickle 1988; White & McKenzie 1989; Wilson 1989). This process commonly produces magmas with OIB-like geochemical characteristics derived from enriched and compositionally heterogeneous mantle domains.

The intraplate extensional character identified in the southern MM can be evaluated in light of Paleozoic tectonomagmatic studies conducted from the Western Carpathians through the ATB to NW Iran and the Iraq segment of the northern Gondwanan (Paleo-Tethyan) margin. Rather than representing a single uniform tectonic regime, these studies describe variable geodynamic settings along this belt.

In the western Carpathians, Early Paleozoic magmatic rocks have been interpreted within an immature back-arc and supra-subduction extensional setting (Putiš et al. 2009). Similarly, metabasic rocks of the Zemplinic Unit are considered to have formed in a back-arc basin environment characterized by MORB–OIB transitional geochemical affinities (Vozárová et al. 2022).

Permian volcanic sequences in the Eastern Alps are interpreted as products of post-orogenic extension and intracontinental rifting following Variscan convergence (Leitner et al. 2024).

Within the ATB, Late Devonian magmatism in the southern MM has been described as within-plate in character (Koralay 2024). Late Paleozoic volcanic rocks in the Binboğa region are likewise interpreted as intraplate magmatism developed during platform-scale extension (Robertson et al. 2021). In contrast, mafic volcanic rocks from the Eastern Taurides have been interpreted to reflect back-arc basin characteristics within a supra-subduction tectonic framework (Çimen 2018).

In NW Iran, Late Devonian–Carboniferous A-type granitoids and associated mafic rocks have been interpreted within extensional tectonic frameworks, although the mechanisms invoked vary among studies. Azizi et al. (2017) relate the magmatism to intracontinental extension and mantle upwelling processes, emphasizing enriched mantle involvement during lithospheric thinning. Mohammadi et al. (2020) highlight mantle source heterogeneity and magma interaction processes developed under extensional conditions rather than derivation from a depleted MORB-type source. Moghadam et al. (2015) interpret bimodal magmatism as reflecting enriched mantle-derived melts subsequently modified by assimilation and fractional crystallization, indicating both source variability and open-system magmatic evolution. Similarly, Jamei et al. (2021) attribute A-type magmatism to enriched mantle parental magmas emplaced in an intraplate extensional regime and variably modified during ascent.

Lamprophyres from Central Iran are interpreted to derive from a metasomatized lithospheric mantle source influenced by earlier subduction processes, although their emplacement occurred within an extensional tectonic regime (Veysi et al. 2023).

Overall, the regional data indicate that Paleozoic magmatism along this segment of the northern Gondwanan margin was largely associated with extensional tectonics, variably expressed as post-orogenic rifting, intracontinental stretching, or supra-subduction back-arc extension. In this context, the intraplate geochemical signature documented in the southern MM fits coherently within a margin-scale extensional framework rather than a typical arc-building, subduction-dominated magmatic system.

Conclusions

Whole-rock geochemical and Sr–Nd isotopic analyses from 14 locations across the southern Menderes Massif reveal that the metabasic rocks of Babadağ (Denizli) consist of amphibolite, garnet amphibolite, and hornblende gabbro, distinguished by their lithological features. Emplaced as sills and stocks within schist units, these rocks locally preserve structural fabrics that record later tectonic deformation. Their geochemical signatures correspond to the alkaline–subalkaline transition, reflecting intraplate magmatism associated with fractional crystallization and modifications of a variably enriched mantle source.

The geochemical and isotopic characteristics indicate derivation from partial melting of an enriched OIB-like mantle source, probably within the garnet–spinel transition zone. This magmatic activity took place in an extensional tectonic setting, aligning with regional models of lithospheric extension along the northern Gondwana margin during Paleo-Tethys evolution. Following emplacement, the rocks underwent tectono-metamorphic overprinting, as recorded by structural fabrics and syn-tectonic garnet growth. However, whether these metamorphic features are linked to an early-stage event or represent a later overprint remains unresolved and requires further investigation.

Amphibolites published by Koralay (2024) from the MM, which is located in a region close to the present study area, exhibit Sr–Nd isotope compositions similar to those of the samples analyzed here, suggesting derivation from a compositionally similar enriched mantle reservoir. However, the metabasic rocks examined in this study are characterized by higher MgO, Ni, Cr, and Mg# values, indicating derivation from less evolved melts and implying relatively higher degrees of mantle melting. These differences are interpreted to reflect local variations in melting conditions rather than fundamentally distinct mantle sources.

Acknowledgements: This research was supported by the Pamukkale University Scientific Research Projects Coordination Unit (Project No. 2021FEBE025) and is part of the corresponding author's doctoral thesis. The authors thank Dr. Tamer Koralay and Dr. Ersin Koralay for guidance and contributions. We thank Elif Meriç İlkimen for participation in the field and laboratory. Special thanks go to Salih Zeki İlkimen for additional vehicle support during fieldwork. We also thank Mehmet Güngör, technical staff in the Department of Geological Engineering at Pamukkale University, for

preparing thin sections. The corresponding author received support from the 'Council of Higher Education – 100/2000 Program' in Computational Science and Engineering and the 'Scientific and Technological Research Council of Türkiye – 2211/A National PhD Scholarship Programs'. The authors would like to thank Managing Editor Dr. Silvia Antolíková for facilitating the communication process during the manuscript review, as well as the anonymous reviewers and Editor-in-Chief Dr. Igor Broska for their constructive comments that improved the manuscript.

References

Abdel-Rahman A.F.M. 2002: Mesozoic volcanism in the Middle East: geochemical, isotopic and petrogenetic evolution of extension–related alkali basalts from central Lebanon. *Geological Magazine* 139, 621–640. https://doi.org/10.1017/S0016756802006829

Abdulzahra I.K., Hadi A., Asahara Y., Azizi H., & Yamamoto K. 2016: Zircon U–Pb ages and geochemistry of Devonian A–type granites in the Iraqi Zagros Suture Zone (Damamna area): New evidence for magmatic activity related to the Hercynian orogeny. *Lithos* 264, 360–374. https://doi.org/10.1016/j.lithos.2016.09.006

Akarsu İ. 1969: Ege Bölgesinin (Babadağ ve civarı) jeolojisi. *Türkiye Jeoloji Bülteni* 12, 1–10.

Aysal N., Öngen S., Peytcheva I. & Keskin M. 2012: Origin and evolution of the Havran Unit, Western Sakarya basement (NW Turkey): new LA-ICP-MS U–Pb dating of the metasedimentary-metagranitic rocks and possible affiliation to Avalonian microcontinent. *Geodinamica Acta* 25, 226–247. https://doi.org/10.1080/09853111.2014.882536

Azizi H., Kazemi T. & Asahara Y. 2017: A–type granitoid in Hasansalaran complex, northwestern Iran: Evidence for extensional tectonic regime in northern Gondwana in the Late Paleozoic: *Journal of Geodynamics* 108, 56–72. https://doi.org/10.1016/j.jog.2017.05.003

Barbot S. & Weiss J.R. 2021: Connecting subduction, extension and shear localization across the Aegean Sea and Anatolia. *Geophysical Journal International* 226, 422–445. https://doi.org/10.1093/gji/ggab078

Bozkurt E. 2007: Extensional v. contractional origin for the southern Menderes shear zone, SW Turkey: tectonic and metamorphic implications. *Geological Magazine* 144(1), 191–210. 10.1017/S0016756806002664

Bozkurt E. & Mittwede S.K. 2001: Introduction to the geology of Turkey – a synthesis. *International Geology Review* 43, 578–594. https://doi.org/10.1080/00206810109465034

Cabanis B. & Lecolle M. 1989: Le diagramme La/10–Y/15–Nb/8: un outil pour la discrimination des séries volcaniques et la mise en évidence des processus de mélange et/ou de contamination crustale. *Comptes Rendus de l'Académie des Sciences* Série 2, 309, 2023–2029.

Candan O., Çetinkaplan M., Oberhänsli R., Rimmelé G. & Akal C. 2005: Alpine high–P/low–T metamorphism of the Afyon Zone and implications for the metamorphic evolution of Western Anatolia, Turkey. *Lithos* 84, 102–124. https://doi.org/10.1016/j.lithos.2005.02.005

Candan O., Dora O.Ö., Oberhänsli R., Koralay O.E., Çetinkaplan M., Akal C., Satır M., Chen F. & Kaya O. 2011a: Stratigraphy of the Pan–African basement of the Menderes Massif and the relationship with late Neoproterozoic/Cambrian evolution of The Gondwana, *Bulletin of the Mineral Research and Exploration* 142, 25–68.

Candan O., Oberhänsli, R., Dora O.Ö., Çetinkaplan M., Koralay O.E., Rimmelé G., Chen F. & Akal C. 2011b: Polymetamorphic evolution of the Pan–African Basement and Palaeozoic–Early tertiary cover series of the Menderes Massif, *Bulletin of the Mineral Research and Exploration* 142, 123–165.

Candan O., Koralay O. E., Topuz G., Oberhänsli R., Fritz H., Collins A.S. & Chen F. 2016: Late Neoproterozoic gabbro emplacement followed by early Cambrian eclogite–facies metamorphism in the Menderes Massif (W. Turkey): Implications on the final assembly of Gondwana. *Gondwana Research* 34, 158–173. https://doi.org/10.1016/j.gr.2015.02.015

Chen W. & Arculus R.J. 1995: Geochemical and isotopic characteristics of lower crustal xenoliths, San Francisco Volcanic Field, Arizona, U.S.A. *Lithos* 36, 203–225. https://doi.org/10.1016/0024-4937(95)00018-6

Çimen 2018: The new findings on the Late Devonian volcanism in the Eastern Taurides (Develi, Kayseri): Preliminary data. *Geological Bulletin of Turkey* 61, 75–90. https://doi.org/10.25288/tjb.358181

Collins A.S. & Robertson A.H. 1999: Evolution of the Lycian Allochthon, western Turkey, as a north–facing Late Palaeozoic to Mesozoic rift and passive continental margin. *Geological Journal* 34, 107–138.

Dora O.Ö. 2011: Historical evolution of the geological researches in the Menderes massif. *Bulletin of the Mineral Research and Exploration* 142, 1–23.

Fitton J.G., James D. & Leeman W.P. 1991: Basic magmatism associated with late Cenozoic extension in the western United States: Compositional variations in space and time. *Journal of Geophysical Research: Solid Earth* 96, 13693–13711. https://doi.org/10.1029/91JB00372

Floyd P.A. & Winchester J.A. 1975: Magma type and tectonic setting discrimination using immobile elements. *Earth and Planetary Science Letters* 27, 211–218. https://doi.org/10.1016/0012-821X(75)90031-X

Göncüoglu M.C. & Kozlu H. 2000: Early Paleozoic evolution of the NW Gondwanaland: data from southern Turkey and surrounding regions. *Gondwana Research* 3, 315–324. https://doi.org/10.1016/S1342-937X(05)70290-2

Göncüoglu M.C. Sayit K. & Tekin U.K. 2010: Oceanization of the northern Neotethys: geochemical evidence from ophiolitic melange basalts within the Izmir–Ankara suture belt, NW Turkey. *Lithos* 116, 175–187. https://doi.org/10.1016/j.lithos.2010.01.007

Gündüz M. & Asan K. 2021: PetroGram: An excel–based petrology program for modeling of magmatic processes. *Geoscience Frontiers* 12, 81–92. https://doi.org/10.1016/j.gsf.2020.06.010

Gürsu S., Möller A., Inglis J.D., Göncüoğlu M.C., Hefferan K., Toksoy–Köksal, F., K. Aynur & Köksal, S. 2023. Tracing the protoliths of the garnet amphibolitic and retrogressed eclogitic slices and a conceptual tectonic model for their emplacement onto the Central Menderes Massif, Turkey: New geochemical data and laser ablation–inductively coupled plasma–mass spectrometry U–Pb zircon and rutile ages. *GSA Bulletin* 135, 2486–2509. https://doi.org/10.1130/B36339.1

Hofmann A.W. 1988: Chemical differentiation of the Earth: the relationship between mantle, continental crust, and oceanic crust. *Earth and Planetary Science Letters* 90, 297–314. https://doi.org/10.1016/0012-821X(88)90132-X

Hofmann A.W. 1997: Mantle geochemistry: the message from oceanic volcanism. *Nature* 385, 219–229. https://doi.org/10.1038/385219a0

Hofmann A.W., Jochum K.P., Seufert M. & White W.M. 1986: Nb and Pb in oceanic basalts: new constraints on mantle evolution. *Earth and Planetary Science Letters* 79, 33–45. https://doi.org/10.1016/0012-821X(86)90038-5

Jamei S., Ghorbani M., Williams I.S. & Moayyed M. 2021: Tethyan oceans reconstructions with emphasis on the Early Carboniferous Pir-Eshagh A–type rhyolite and the Late Palaeozoic magmatism in Iran. *International Geology Review* 63, 1389–1405. https://doi.org/10.1080/00206814.2020.1768443

Janoušek V., Farrow C.M. & Erban V. 2006: Interpretation of whole–rock geochemical data in igneous geochemistry: Introducing Geochemical Data Toolkit (GCDkit). *Journal of Petrology* 47, 1255–1259. https://doi.org/10.1093/petrology/egl013

Köksal S. 2019: The Upper Cretaceous intrusive rocks with extensive crustal contribution in Hacımahmutuşağı Area (Aksaray/Turkey). *Geologica Carpathica* 70, 261–276. https://doi.org/10.2478/geoca-2019-0015

Konak N. & Şenel M. 2002: *Geological map of Türkiye, Denizli quadrangle 1:500.000 scale*. General Directorate of Mineral Research and Exploration, Ankara.

Koralay O.E. 2024: Geochemistry and zircon U–Pb dating of amphibolite in the Menderes Massif (western Türkiye): first record of Late Devonian extension. *International Geology Review* 66, 2195–2215. https://doi.org/10.1080/00206814.2023.2273376

Koralay O.E., Candan O., Akal C., Dora O.Ö., Chen F., Satır M. & Oberhänslı R. 2011: The geology and geochronology of the Pan–African and Triassic metagranitoids in the Menderes Massif, Western Anatolia, Turkey. *Bulletin of the Mineral Research and Exploration* 142, 69–119.

Koralay O.E., Candan O., Chen, F., Akal C., Oberhänsli R., Satır M. & Dora O.Ö. 2012: Pan–African magmatism in the Menderes Massif: geochronological data from leucocratic tourmaline orthogneisses in western Turkey. *International Journal of Earth Sciences* 101, 2055–2081. https://doi.org/10.1007/s00531-012-0775-2

Leake B.E. 1964: The chemical distinction between ortho- and paraamphibolites. *Journal of Petrology* 5, 238–254. https://doi.org/10.1093/petrology/5.2.238

Leitner C., Hauzenberger C.A., Gilg H.A., Friedl G., Von Hagke C. & Finger F. 2024: The geochemical character of synsedimentary volcanism in the Permian Haselgebirge Formation of the Eastern Alps (Austria): Implications for paleogeographic models. *Geologica Carpathica* 75, 359–374. https://doi.org/10.31577/GeolCarp.2024.22

Mackintosh P.W. & Robertson A.H. 2012: Late Devonian–Late Triassic sedimentary development of the central Taurides, S Turkey: implications for the northern margin of Gondwana. *Gondwana Research* 21, 1089–1114. https://doi.org/10.1016/j.gr.2011.07.016

McKenzie D. & Bickle M.J. 1988: The volume and composition of melt generated by extension of the lithosphere. *Journal of Petrology* 29, 625–679. https://doi.org/10.1093/petrology/29.3.625

Moghadam H.S., Li X.H., Ling X.X., Stern R.J., Santos, J.F. Meinhold G., Ghorbani G. & Shahabi S. 2015: Petrogenesis and tectonic implications of Late Carboniferous A-type granites and gabbronorites in NW Iran: Geochronological and geochemical constraints. *Lithos* 212, 266–279. https://doi.org/10.1016/j.lithos.2014.11.009

Mohammadi A., Moazzen M., Lechmann A. & Laurent O. 2020: Zircon U–Pb geochronology and geochemistry of Late Devonian–Carboniferous granitoids in NW Iran: implications for the opening of Paleo–Tethys. *International Geology Review* 62, 1931–1948. https://doi.org/10.1080/00206814.2019.1675540

Oberhänsli R., Candan O. & Wilke F. 2010: Geochronological Evidence of Pan–African Eclogites from The Central Menderes Massif, Turkey. *Turkish Journal of Earth Sciences* 19, 431–447. https://doi.org/10.3906/yer-1001-20

Okay A.I. 2001: Stratigraphic and metamorphic inversions in the central Menderes Massif: A new structural model. *International Journal of Earth Sciences* 91, 173–178. https://doi.org/10.1007/s005310000098

Okay A.I. 2008: Geology of Turkey: a synopsis. *Anschnitt* 21, 19–42.

Okay A.I. 2011: Tavşanlı Zone: The Northern Subducted Margin of the Anatolide–Tauride Block. *Bulletin of the Mineral Research and Exploration* 142, 191–221.

Okay A.I. & Nikishin A.M. 2015: Tectonic evolution of the southern margin of Laurasia in the Black Sea region. *International Geology Review* 57, 1051–1076. https://doi.org/10.1080/00206814.2015.1010609

Okay A.I. & Tüysüz O. 1999: Tethyan sutures of northern Turkey. *Geological Society, London, Special Publications* 156, 475–515. https://doi.org/10.1144/GSL.SP.1999.156.01.22

Okay A.I., Satir M. & Siebel W. 2006: Pre–Alpide Palaeozoic and Mesozoic orogenic events in the Eastern Mediterranean region. In: Gee D.G. & Stephenson R.A. (Eds.): *European Lithosphere Dynamics*. Geological Society, London, 389–485. https://doi.org/10.1144/GSL.MEM.2006.032.01.23

Özer S., Sözbilir H., Özkar İ., Toker V. & Sari B. 2001: Stratigraphy of Upper Cretaceous–Palaeogene sequences in the southern and eastern Menderes Massif (western Turkey). *International Journal of Earth Sciences* 89, 852–866. https://doi.org/10.1007/s005310000142

Pearce J.A. 1982: Trace element characteristics of lavas from destructive plate boundaries. In: Thorpe R.S. (Ed.): *Andesites: Orogenic Andesites and Related Rocks*. John Wiley & Sons, Chichester, 525–548.

Pearce J.A. 1983: Role of the sub–continental lithosphere in magma genesis at active continental margins. In: Hawkesworth C.J. & Norry M.J. (Eds.): *Continental Basalts and Mantle Xenoliths*. Shiva Publications, Nantwich, Cheshire, 230–249.

Pearce J.A. 1996: A user's guide to basalt discrimination diagrams. In: Wyman D.A. (Ed.): *Trace Element Geochemistry of Volcanic Rocks: Applications for Massive Sulphide Exploration*. Geological Association of Canada, *Short Course Notes* 12, 79–113.

Pearce J.A. 2008: Geochemical fingerprinting of oceanic basalts with applications to ophiolite classification and the search for Archean oceanic crust. *Lithos* 100, 14–48. https://doi.org/10.1016/j.lithos.2007.06.016

Putiš M., Ivan P., Kohút M., Spišiak J., Siman P., Radvanec M., Uher P., Sergeev S., Larionov A., Méres Š., Demko R. & Ondrejka M. 2009: Meta-igneous rocks of the West–Carpathian basement, Slovakia: indicators of Early Paleozoic extension and shortening events. *Bulletin de la Société géologique de France* 180, 461–471. https://doi.org/10.2113/gssgfbull.180.6.461

Rimmelé G., Jolivet L., Oberhänsli R. & Goffé B. 2003a: Deformation history of the high–pressure Lycian Nappes and implications for tectonic evolution of SW Turkey. *Tectonics* 22. https://doi.org/10.1029/2001TC901041

Rimmelé G., Oberhänsli R., Goffé B., Jolivet L., Candan O. & Çetinkaplan M. 2003b: First evidence of high–pressure metamorphism in the "Cover Series" of the southern Menderes Massif. Tectonic and metamorphic implications for the evolution of SW Turkey. *Lithos* 71, 19–46. https://doi.org/10.1016/S0024-4937(03)00089-6

Ring U., Gessner K., Güngör T. & Passchier C.W. 1999: The Menderes Massif of western Turkey and the Cycladic Massif in the Aegean – do they really correlate?. *Journal of the Geological Society* 156, 3–6. https://doi.org/10.1144/gsjgs.156.1.0003

Robertson A.H.F. & Dixon J.E. 1984: Introduction: aspects of the geological evolution of the Eastern Mediterranean. *Geological Society London, Special Publications* 17, 1–74. https://doi.org/10.1144/GSL.SP.1984.017.01.02

Robertson A.H., Parlak O. & Ustaömer T. 2021: Late Palaeozoic extensional volcanism along the northern margin of Gondwana in southern Turkey: implications for Palaeotethyan development. *International Journal of Earth Sciences* 110, 1961–1994. https://doi.org/10.1007/s00531-021-02051-7

Rollinson H.R. 1993: *Using geochemical data: evaluation, presentation, interpretation*. Longman Scientific and Technical, Wiley, New York, 1–352.

Saccani E. 2015: A new method of discriminating different types of post–Archean ophiolitic basalts and their tectonic significance using Th–Nb and Ce–Dy–Yb systematics. *Geoscience Frontiers* 6, 481–501. https://doi.org/10.1016/j.gsf.2014.03.006

Schmid S.M., Fügenschuh B., Kounov A., Maţenco L., Nievergelt P., Oberhänsli R., Jan P., Senecio S., Ralf S., Bruno T., Kamil U. & van Hinsbergen D.J. 2020: Tectonic units of the Alpine collision zone between Eastern Alps and western Turkey. *Gondwana Research* 78, 308–374. https://doi.org/10.1016/j.gr.2019.07.005

Şengör A.M.C. 1984: The Cimmeride Orogenic System and the Tectonics of Eurasia. *Geological Society of America Special Paper* 195, 1–74. https://doi.org/10.1130/SPE195-p1

Şengör A.M.C. & Yilmaz Y. 1981: Tethyan evolution of Turkey: A plate tectonic approach. *Tectonophysics* 75, 181–241. https://doi.org/10.1016/0040-1951(81)90275-4

Şengör A.M.C., Satir M. & Akkök R. 1984a: Timing of tectonic events in the Menderes Massif, western Turkey: Implications for tectonic evolution and evidence for Pan-African basement in Turkey. *Tectonics* 3, 693–707. https://doi.org/10.1029/TC003i007p00693

Şengör A.M.C., Yılmaz Y. & Sungurlu O. 1984b: Tectonics of the Mediterranean Cimmerides: nature and evolution of the western termination of Palaeo-Tethys. *Geological Society, London, Special Publications* 17, 77–112. https://doi.org/10.1144/GSL.SP.1984.017.01.04

Şengör A.C., Altıner D., Zabcı C., Sunal G., Lom N., Aylan E. & Öner T. 2023: On the nature of the Cimmerian Continent. *Earth-Science Reviews* 247, 104520. https://doi.org/10.1016/j.earscirev.2023.104520

Shervais J.W. 2022: The petrogenesis of modern and ophiolitic lavas reconsidered: Ti–V and Nb–Th. *Geoscience Frontiers* 13, 101319. https://doi.org/10.1016/j.gsf.2021.101319

Smith E.I., Sánchez A., Walker J.D. & Wang K. 1999: Geochemistry of mafic magmas in the Hurricane Volcanic field, Utah: implications for small-and large-scale chemical variability of the lithospheric mantle. *The Journal of Geology* 107, 433–448. https://doi.org/10.1086/314355

Stampfli G.M. & Borel G.D. 2002: A plate tectonic model for the Paleozoic and Mesozoic constrained by dynamic plate boundaries and restored synthetic oceanic isochrons. *Earth and Planetary Science Letters* 196, 17–33. https://doi.org/10.1016/S0012-821X(01)00588-X

Stampfli G.M., Hochard C., Vérard C., Wilhem C. & von Raumer J. 2013: The formation of Pangea. *Tectonophysics* 593, 1–19. https://doi.org/10.1016/j.tecto.2013.02.037

Sun S.S. & McDonough W.F. 1989: Chemical and isotopic systematics of oceanic basalts: implications for mantle composition and processes. *Geological Society, London, Special Publications* 42, 313–345. https://doi.org/10.1144/GSL.SP.1989.042.01.19

Topuz G., Candan O., Okay A.I., von Quadt A., Othman M., Zack T. & Wang J. 2020: Silurian anorogenic basic and acidic magmatism in Northwest Turkey: Implications for the opening of the Paleo-Tethys. *Lithos* 356, 105302. https://doi.org/10.1016/j.lithos.2019.105302

van Hinsbergen D.J., Torsvik T.H., Schmid S.M., Maţenco L.C., Maffione M., Vissers R.L.M.., Gürer D. & Spakman W. 2020: Orogenic architecture of the Mediterranean region and kinematic reconstruction of its tectonic evolution since the Triassic. *Gondwana Research* 81, 79–229. https://doi.org/10.1016/j.gr.2019.07.009

Veysi S., Manesh S.M.T., Shirdashtzadeh N. & Francisco J.S. 2023: Paleozoic Tensional Intraplate Magmatism and Mantle Evolution in Central Iran Zone: Geochemistry, Nd–Sr Isotope Data of Lamprophyres. *Petrology* 31, 459–474. https://doi.org/10.1134/S0869591123040082

Vozárová A., Nemec O., Šarinová K. & Vozár J. 2022: Metabasic rocks from the Zemplinic crystalline basement (Western Carpathians, Slovakia): Metamorphic evolution and igneous protolith. *Geologica Carpathica* 73, 599–616. https://doi.org/10.31577/GeolCarp.73.6.6

Whitney D.L. & Evans B.W. 2010: Abbreviations for names of rock-forming minerals. *American mineralogist* 95, 185–187. https://doi.org/10.2138/am.2010.3371

White R. & McKenzie D. 1989: Magmatism at rift zones: the generation of volcanic continental margins and flood basalts. *Journal of Geophysical Research: Solid Earth 94*, 7685–7729.

Wilson B.M. 1989: *Igneous petrogenesis a global tectonic approach*. Department of Earth sciences. Chapman & Hall, 1–466.

Yılmaz İ., Dursun G., Akgündüz S., Laçin D., Tükel-Şişman F. & Sert B. 2025: Maximum depositional age, provenance, and paleogeographic evolution of the Early Paleozoic succession of the Istanbul Zone: Insights from detrital zircon U–Pb geochronology and geochemistry. *Geologica Carpathica* 76, 391–416. https://doi.org/10.31577/GeolCarp.2025.23

Zindler A. & Hart S. 1986: Chemical geodynamics. *Annual Review of Earth and Planetary Sciences* 14, 493–571. https://doi.org/10.1146/annurev.ea.14.050186.002425

Zlatkin O., Avigad D. & Gerdes A. 2013: Evolution and provenance of Neoproterozoic basement and Lower Paleozoic siliciclastic cover of the Menderes Massif (western Taurides): coupled U–Pb–Hf zircon isotope geochemistry. *Gondwana Research* 23, 682–700. https://doi.org/10.1016/j.gr.2012.05.006

Electronic supplementary material is available online:

Supplementary Table S1 at https://geologicacarpathica.com/data/files/supplements/GC-77-3-Colak_TableS1.xlsx
Supplementary Table S2 at https://geologicacarpathica.com/data/files/supplements/GC-77-3-Colak_TableS2.xlsx
Supplementary Table S3 at https://geologicacarpathica.com/data/files/supplements/GC-77-3-Colak_TableS3.xlsx